An Experimental Evaluation of GNSS/INS Verification Strategies for Vehicular Applications

Daniele Borio
European Commission, Joint Research Centre (JRC),
Via Enrico Fermi 2749, 21027 Ispra (VA), Italy
Email: daniele.borio@ec.europa.eu

***Abstract*—An effective way to detect the presence of a spoofing attack is to verify Global Navigation Satellite System (GNSS) data with measurements from other sensors, such as Inertial Navigation Systems (INSs). In this paper, uncoupled GNSS/INS verification approaches are experimentally evaluated in an automotive context. The approaches are uncoupled in the sense that GNSS and INS sensors are operated independently without exchange of information. The approaches considered are the Magnitude Verification (MAV) technique, where the acceleration and angular velocity magnitudes are compared, and the Horizontal Components (HoC) verification strategy that requires vertical alignment of the GNSS and INS sensor frames.**
The analysis shows the effectiveness of this type of approaches and discusses their limitations, for example in low dynamic conditions, when low accelerations and angular velocities are recorded. Possible enhancements are also discussed.

***Index Terms*—acceleration, angular velocity, GNSS, inertial sensors, spoofing detection**

I. Introduction

Global Navigation Satellite System (GNSS) spoofing is an emerging threat where the Position, Velocity and Timing (PVT) information provided by a GNSS receiver is falsified [1]. In safety applications, such as the Smart Tachograph (ST) [2], [3], the legislator has mandated the adoption of verification methods where GNSS information is cross-checked against measurements from other sensors [4]. The potentially severe impact of GNSS spoofing has motivated significant research work towards the development of techniques for data verification. A schematic representation of some of the techniques adopted in the vehicular and transportation sector is provided in Fig. 1. These approaches can be divided in two major classes: i) coupled [5], [6], [7] and ii) uncoupled [8], [9]. In the first class of approaches, GNSS and Inertial Navigation System (INS) data are integrated in a single navigation solution using, for example, an Extended Kalman Filter. As part of the integrated navigation algorithm, the innovation sequences are computed. Innovations reflect the conformance of the different measurements with the position solution and the underling model used for its computation. If the innovations associated to the inertial measurements are too large, then the presence of a spoofing attack is declared. In this type of approaches, measurements from different sensors are coupled for the computation of a single position solution.
A second class of spoofing detection algorithms, denoted here as uncoupled techniques, performs data comparison in the domain of the inertial measurements. In this case, GNSS and INS measurements are uncoupled and used in an independent way. The GNSS PVT solution is used to compute accelerations and angular velocities that can be compared with the output of the inertial unit. In order to perform a comparison between GNSS and INS data, it is necessary to express the measurements in the same reference frame. For this reason, [9] proposed a strategy based on the acceleration and angular velocity magnitude that is conserved between different reference frames. This method is denoted here as Magnitude Verification (MAV). The authors of [8] exploited the dynamic model of a plane to extract the vertical acceleration from the Inertial Measurement Unit (IMU) and compared it with the vertical acceleration obtained from the GNSS receiver. In this case, measurements from the gyroscopes were not used.
In this paper, an experimental evaluation of uncoupled GNSS/INS verification strategies is provided involving different types of sensors and scenarios. In addition to the MAV approach, a second strategy requiring vertical alignment, i.e. levelling, is proposed. The technique proposed adapts the approach described in [8] to vehicular applications and introduces an additional verification based on the horizontal angular velocity.
The paper shows the effectiveness of this type of approaches and discusses their limitations, for example in low dynamic conditions, when low accelerations and low angular velocities

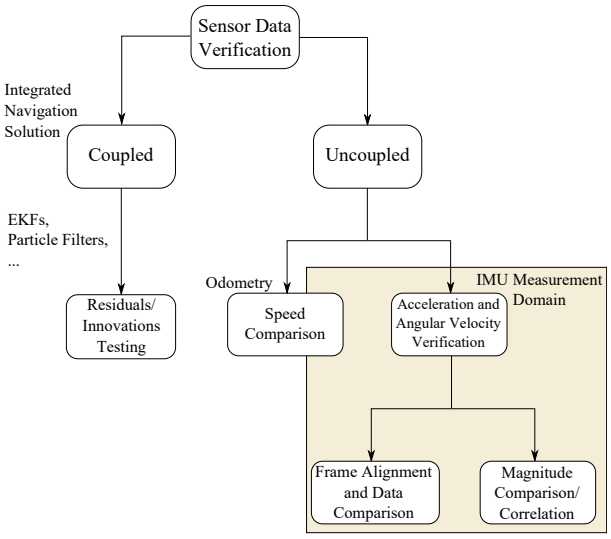

Fig. 1. Different GNSS and sensor data verification strategies.

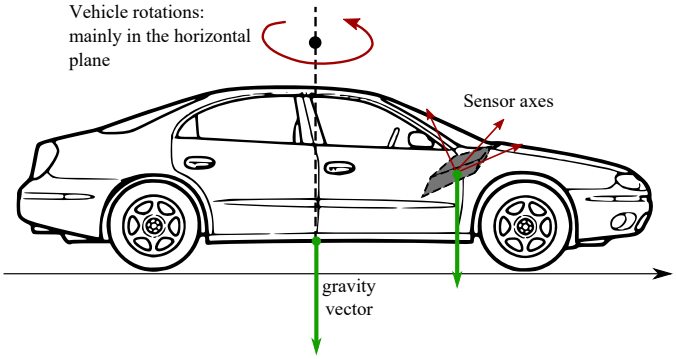

Fig. 2. Relative orientation between the vehicle and the IMU.

are recorded. Possible enhancements are then discussed.

II. Data Verification Strategies

In the techniques considered in this paper, some basic assumptions are made with respect to the vehicle dynamics and sensor orientation. In particular, the configuration shown in Fig. 2 is assumed: the IMU is steadily attached to the vehicle and the sensor orientation is constant with respect to the vehicle frame. Moreover, it is assumed that the vertical displacement of the vehicle is negligible and that it rotates only around its vertical axis. The accelerations provided by the IMU are affected by gravity whose effect should be removed for the comparison with GNSS measurements. In [9], this operation is performed using a high-pass filter. A different approach is considered in Section II-D, where the gravity vector is at first estimated and used to align the vertical axis of the IMU.
The model depicted in Fig. 2 is commonly adopted in the literature to design spoofing verification algorithms.

A. Magnitude Verification

The MAV algorithm proposed by [9] considers only the magnitude of the accelerations and of the angular velocities. For this reason, there is no need to align the sensor frame with the local East North Up (ENU) frame employed to represent the measurements provided by the GNSS receiver. The approach is composed of two parts. The first part is required for the processing of the GNSS measurements whereas the second processing block is adopted for the IMU data. The two parts are depicted in Fig. 3 that provides a schematic representation of the MAV algorithm. The processing adopted for the GNSS measurements is depicted in the upper part of Fig. 3. The input to the algorithm is the GNSS velocity vector in a local ENU frame. In the original version of the MAV algorithm, the GNSS-derived position vector at time nT_s was used as input. T_s is the sampling interval of the measurements and n is the time index. This vector was then differenced twice using two first order digital differentiators. While this approach is valid, it is also possible to use the velocity vector directly provided by the GNSS receiver and denoted here as $\overrightarrow{v}_G = [v_E, v_N, v_U]^T$ with v_E, v_N and v_U the three velocity components expressed in a local ENU frame. Velocity components are computed using Doppler measurements and are usually accurate at the decimetre/second level [10, p. 621]. Moreover, the use of the velocity vector avoids double differentiation. Digital differentiators are high-pass filters that tend to enhance high frequency noise. The components of the velocity vector, $\overrightarrow{v}_G[n]$, are differentiated once using the a digital differentiator with transfer function:

$$H_\Delta(z) = \frac{1 - z^{-1}}{T_s}. \tag{1}$$

In this way, the GNSS-derived acceleration is obtained:

$$\overrightarrow{a}_G[n] = \begin{bmatrix} a_E[n] \\ a_N[n] \\ a_U[n] \end{bmatrix} = \frac{1}{T_s} \begin{bmatrix} v_E[n] - v_E[n-1] \\ v_N[n] - v_N[n-1] \\ v_U[n] - v_U[n-1] \end{bmatrix}. \tag{2}$$

The GNSS-derived acceleration vector, $\overrightarrow{a}_G[n]$, will be used also by the Horizontal Components (HoC) verification method detailed in the next section. In this respect, the two methods share similar processing schemes for the GNSS signals.
The MAV method only uses the acceleration magnitude that is computed as

$$a_G[n] = \|a_G[n]\|_2 = \sqrt{a_E^2[n] + a_N^2[n] + a_U^2[n]}. \tag{3}$$

GNSS velocity components are also used to estimate the angular velocity that is obtained by differentiating the estimated heading:

$$\omega_z^G[n] = \frac{1}{T_s}\left[\arctan\left(\frac{v_E[n]}{v_N[n]}\right) - \arctan\left(\frac{v_E[n-1]}{v_N[n-1]}\right)\right]. \tag{4}$$

Using the assumption that the vehicle rotates only around its vertical axis, the vector with the angular velocities has a single component, $\omega_z^G[n]$, and its norm is given by

$$\omega_a^G[n] = |\omega_z^G[n]|. \tag{5}$$

The processing applied to the IMU measurements is summarized in the bottom part of Fig. 3. The gravity vector is at first estimated and then removed from the accelerometer measurements. In [9], gravity is removed using an high-pass filter. This is equivalent to estimate gravity using the complementary low-pass filter. This approach is commonly used in the literature to separate the acceleration due to gravity and to actual motion [11]. An approach based on the model assumption made at the beginning of the paper is discussed in Section II-D.
After removing the gravity component, the norm of the IMU acceleration vector is computed and $a_I[n]$ is obtained. $a_I[n]$ is then compared with $a_G[n]$ obtained from the GNSS measurements.
The absolute angular velocity, $\omega_a[n]$, is computed directly as the norm of the gyroscope measurements, $\overrightarrow{\omega}_a[n]$. As for the absolute acceleration, $\omega_a[n]$ is compared with $\omega_a^G[n]$.
The four signals $a_I[n]$, $a_G[n]$, $\omega_a[n]$ and $\omega_a^G[n]$ are used to compute the final decision statistics used to verify the consistency between GNSS and INS time series.

B. Horizontal Components Verification

The HoC verification strategy is obtained by modifying the approach described in [8] that was originally proposed for avionic applications and exploits the dynamic properties

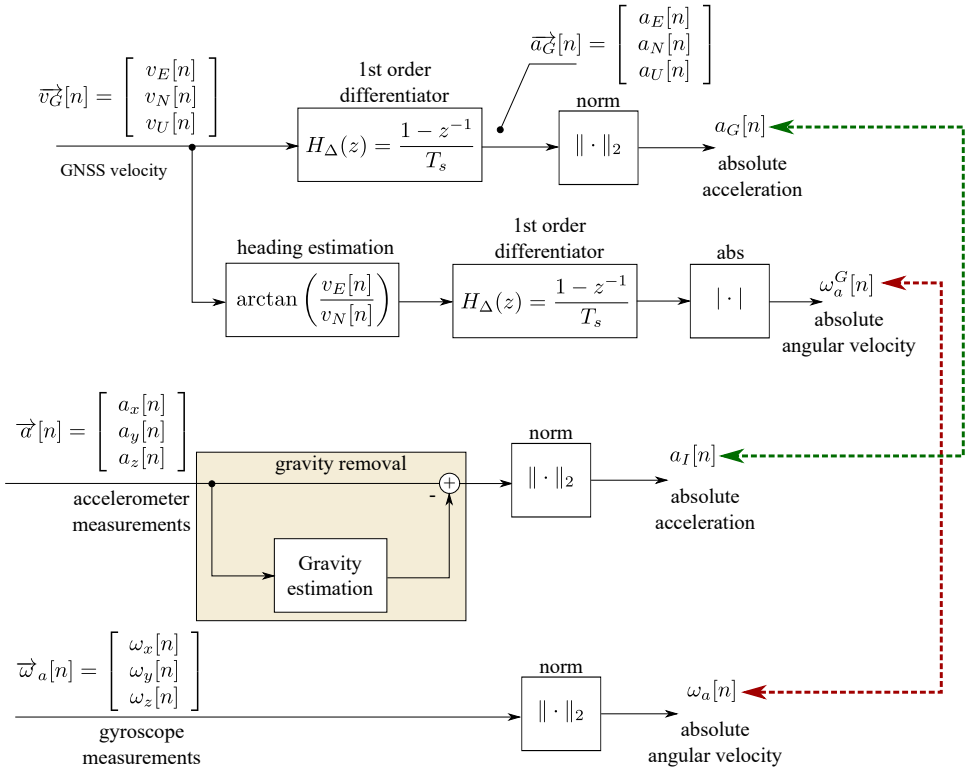

Fig. 3. Schematic representation of the algorithm proposed by [9]. Only the norms of the accelerations and of the angular velocities are considered.

of aeroplane motions. The HoC approach also introduces the use of angular velocity measurements from gyroscopes. These measurements were not considered in [8] that used only accelerations.

Differently from the MAV approach, the HoC technique aligns the IMU frame with the local gravity vector. The gravity vector, $\overrightarrow{g}[n]$ is at first estimated from the IMU measurements and used to determine the rotation matrix, $\mathbf{R}_g[n]$, that rotates the IMU measurements such that, in the new frame, $\overrightarrow{g}[n]$ is aligned with the vertical axis. This process is also called levelling. In this way, the rotated acceleration vector:

$$\overrightarrow{a}^{\,g}[n] = \begin{bmatrix} a_x^g[n] \\ a_y^g[n] \\ a_z^g[n] \end{bmatrix} = \mathbf{R}_g[n]\overrightarrow{a}[n] = \mathbf{R}_g[n] \begin{bmatrix} a_x[n] \\ a_y[n] \\ a_z[n] \end{bmatrix} \quad (6)$$

is obtained. $\overrightarrow{a}[n]$ is the acceleration vector provided by the IMU. When the gravity vector is properly estimated, the gravity acceleration component is contained in $a_z^g[n]$ that is discarded. The horizontal components, $a_x^g[n]$ and $a_y^g[n]$ are retained and used to compute the horizontal acceleration:

$$a_h[n] = \sqrt{(a_x^g[n])^2 + (a_y^g[n])^2}. \quad (7)$$

The IMU horizontal acceleration is compared to the corresponding acceleration computed from the GNSS-derived time series, $a_E[n]$ and $a_N[n]$. The horizontal acceleration computed from GNSS measurements is denoted here as $a_h^G[n]$.

When $\mathbf{R}_g[n]$ is applied to the angular velocity vector, $\overrightarrow{\omega}_a[n]$, the horizontal components of the rotated vector, $\omega_x^g[n]$ and $\omega_y^g[n]$, should contain only noise and residual errors. This is due to the hypothesis discussed at the beginning of this section

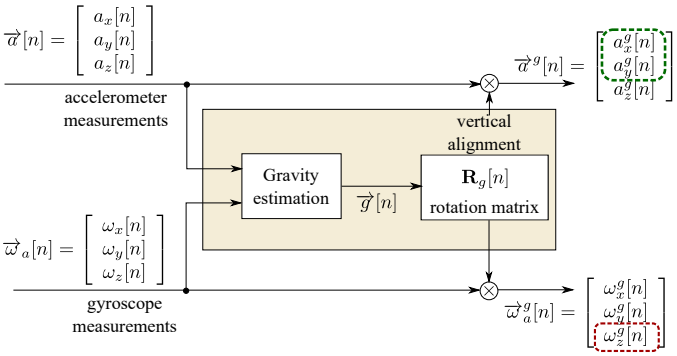

Fig. 4. Schematic representation of the HoC verification algorithm. The gravity vector is estimated and used to align the sensor measurements.

that rotations should occur only around the vertical axis. For this reason, only $\omega_z^g[n]$ is retained and directly compared with $\omega_z^G[n]$. A schematic representation of the processing adopted by the HoC approach for IMU measurements is provided in Fig. 4. The decision statistics for the HoC approach are better discussed in the next section.

C. Decision Statistics

Several approaches can be adopted to compare time series and form the final decision statistics. In this paper, the approach proposed by [9] is adopted and the decision statistics are based on the correlation coefficient, which is defined for

two time series, $x[n]$ and $y[n]$, as:

$$C(x[n], y[n]) = \frac{\frac{1}{N}\sum_{i=0}^{N}(x[n-i] - \bar{x}[n])(y[n-i] - \bar{y}[n])}{\sigma_x[n]\sigma_y[n]} \tag{8}$$

where $\bar{x}[n]$ and $\bar{y}[n]$ are the sample mean of $x[n]$ and of $y[n]$. $\sigma_x[n]$ and $\sigma_y[n]$ are the corresponding sample standard deviations. In practice, an analysis window is used to select N samples from $x[n]$ and $y[n]$. These samples are then used to estimate the means and standard deviations of $x[n]$ and $y[n]$ and to compute the correlation coefficient, $C(x[n], y[n])$.
Four decision statistics are obtained, two for the MAV approach and two for the HoC verification strategy:

$$\begin{aligned} M_{acc}[n] &= C(a_I[n], a_G[n]), \\ M_{ag}[n] &= C(\omega_a[n], \omega_a^G[n]), \\ H_{acc}[n] &= C(a_h[n], a_h^G[n]), \\ H_{ag}[n] &= C(\omega_z^g[n], \omega_z^G[n]). \end{aligned} \tag{9}$$

Each pair of decision statistics can be combined to determine the final quantities used for detecting inconsistencies between time series. In the following, the four decision statistics defined in (9) are analysed separately.

D. Gravity estimation

The MAV and HoC approaches require gravity estimation. The first to remove the gravity vector from the accelerometer measurements, the second for levelling. Several approaches exist for gravity estimation [11], [12], [13]. In this paper, a gradient descent algorithm has been developed based on the model assumptions described at the beginning of this section. According to the model described above, the acceleration sensed by the IMU along the vehicle vertical axis should be closed to the gravity vector,

$$\overrightarrow{g}[n] = g\,\overrightarrow{u}_g[n] \tag{10}$$

where $\overrightarrow{u}_g[n]$ is the unit vector associated to $\overrightarrow{g}[n]$ and g is the gravity constant. $\overrightarrow{g}[n]$ and $\overrightarrow{a}[n]$ are expressed in the same reference frame and, ideally

$$\langle \overrightarrow{a}[n], \overrightarrow{u}_g[n] \rangle = g \tag{11}$$

where $\langle \cdot, \cdot \rangle$ denotes scalar product. The angular velocity should also be concentrated on the horizontal plane and the magnitude of the scalar product

$$\langle \overrightarrow{\omega}_a[n], \overrightarrow{u}_g[n] \rangle \tag{12}$$

should be maximized by $\overrightarrow{u}_g[n]$. For this reason, the following cost function

$$J(\overrightarrow{u}_g[n]) = (\langle \overrightarrow{a}[n], \overrightarrow{u}_g[n] \rangle - g)^2 - w(\langle \overrightarrow{\omega}_a[n], \overrightarrow{u}_g[n] \rangle)^2 \tag{13}$$

has been introduced. $\overrightarrow{u}_g[n]$ is determined by minimizing $J(\overrightarrow{u}_g[n])$ under the constraint $\|\overrightarrow{u}_g[n]\|_2 = 1$. w is a constant that determines the relative weighting between accelerometer and gyroscope contributions. The minimization of $J(\overrightarrow{u}_g[n])$ has been obtained using a gradient descent algorithm [14] where the additional term

$$\lambda(\|\overrightarrow{u}_g[n]\|_2^2 - 1)^2 \tag{14}$$

was incorporated into the cost function to enforce the normalization condition on $\overrightarrow{u}_g[n]$. λ is a constant set to an arbitrary large value.

III. Experimental Setup

In order to experimentally evaluate the effectiveness of the two approaches described in Section II, several data collections were performed using different types of IMUs. All the data collections were performed in a road environment with the IMU steadily attached to the vehicle used for the test. The devices used for the tests were:

- a high-end NovAtel SPAN-CPT system integrating Fiber Optic Gyros (FOG) gyroscopes and Micro Electro-Mechanical Systems (MEMS) accelerometers. The IMU integrated within the SPAN-CPT system is considered of good quality.
- two ublox M8U units with Dead Reckoning (DR) sensors. The IMUs integrated within the ublox receivers are considered of medium quality.
- a Huawei P10 smartphone with low-cost MEMS accelerometers and gyroscopes.
- a low-cost Huawei G Play mini smarthphone with inertial units of poor quality. This device is used to show the limits of the techniques considered.

A view of the experimental setup adopted for testing the GNSS/IMU verification strategies using the SPAN-CPT system is provided in Fig. 5. The SPAN-CPT system was placed on the back of the car. A second GNSS receiver, a ublox M8T device was connected through an Radio Frequency (RF) splitter to the same antenna used for the SPAN-CPT system. The position/velocity solution provided by the ublox M8T receiver was compared with the inertial data provided by the SPAN-CPT system. This choice was adopted to avoid coupling between the position solution provided by the SPAN-CPT system and the inertial measurements.
The tests performed using the SPAN-CPT system were conducted inside the Joint Research Centre (JRC) campus in Ispra, Italy. Several loops were performed on the trajectory shown in Fig. 5a) and, in total, more than 4 hours of data were collected. The experimental setup adopted for the tests involving the ublox M8U receivers and the smartphones is shown in Fig. 6. The internal views of the two vehicles used for these tests are shown in Figs. 6a) and b), respectively. Most of the tests were performed in highway environments. One of the trajectory performed during the tests is shown in Fig. 6c). In order to avoid coupling between GNSS and IMU data, raw GNSS measurements from the ublox receiver were adopted to compute the vehicle PVT without inertial measurements. This PVT solution was used as comparison term for all the three devices used for testing.
In order to analyse the behaviour of the decision statistics in the presence of a spoofing attack, a simple meaconing scenario was simulated. Unrelated GNSS and inertial measurements from different data collections were compared. This corresponds to a replay attack where old GNSS data are replayed and compared with unrelated IMU measurements. This is the same approach used in [9] to analyse the MAV approach.

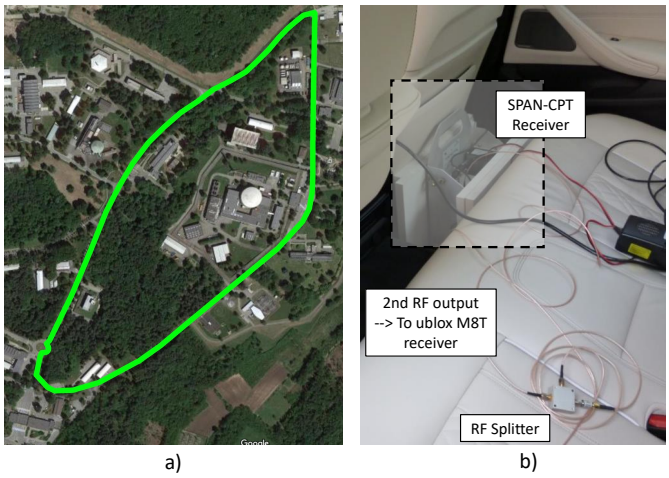

Fig. 5. Experimental setup adopted for testing GNSS/INS verification strategies using the SPAN-CPT system. a) Trajectory selected for the tests. b) Internal view of the vehicle with the SPAN-CPT system.

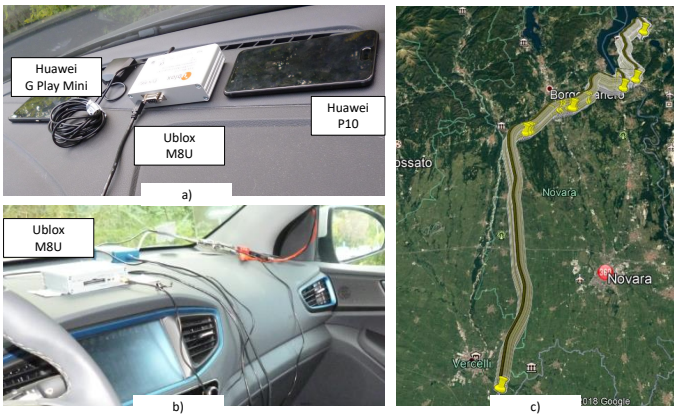

Fig. 6. Experimental setup used to test GNSS/INS verification strategies using smartphones and ublox M8U receivers. a) Internal view of the first vehicle. b) Internal view of the second vehicle. c) Trajectory of one of the tests performed.

IV. Experimental Results

A. SPAN-CPT IMU

Results obtained for the SPAN-CPT unit are presented first. The time series, $a_h[n]$, $a_h^G[n]$, $\omega_z^g[n]$ and $\omega_z^G[n]$ obtained using the SPAN-CPT system are provided in Fig. 7 for the scenario illustrated in Fig. 5 a). After an initial period during which the vehicle was static, the driver performed several loops in a roundabout. This part of the test can be clearly identified from the angular velocity plot in the bottom part of Fig. 7 where an almost constant angular velocity can be observed. After these initial phases, the vehicle performed several times the closed trajectory illustrated in Fig. 5 a).

A good agreement between GNSS and IMU data can be observed. The two sensors provide similar information and correct validation can be performed. This fact clearly emerges from Fig. 8 that provides the four decision statistics obtained using the SPAN-CPT data. The test statistics have been computed using an analysis window of 120 seconds. For most of the duration of the experiment, the correlation coefficients assume values above 0.8 showing the high level of correlation

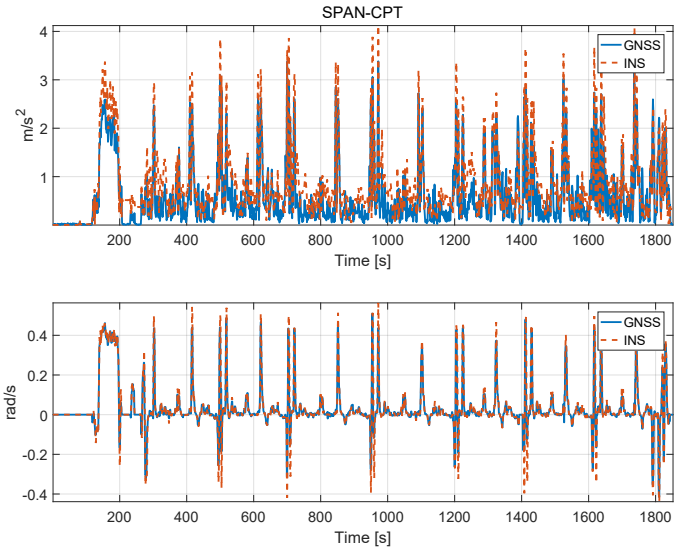

Fig. 7. Comparison between time series obtained using the HoC approach. Upper part) Horizontal acceleration. Bottom part) Angular velocity. SPAN-CPT experiment, genuine scenario.

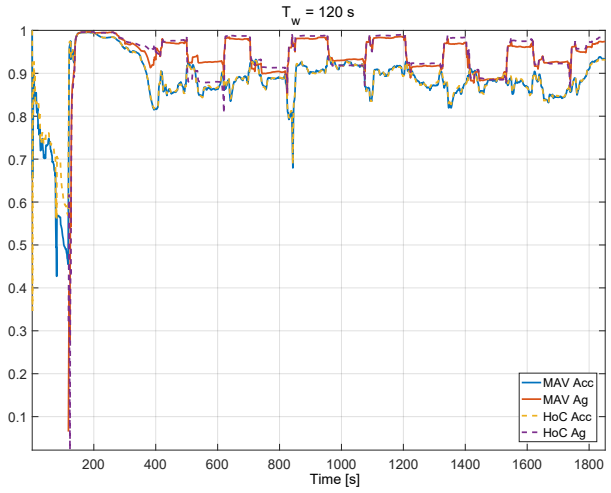

Fig. 8. Decision statistics computed for the SPAN-CPT scenario analysed in Fig. 7.

between GNSS and IMU data. The decision statistics assume lower values only at the beginning of the test when the vehicle is static. Under these conditions and for low accelerations, it is not possible to cross-validate the sensor data as further discussed in Section V-A.

In this case, the decision statics obtained using angular velocity measurements (indicated by the subscript 'Ag' in Fig. 8) assume higher values than the corresponding acceleration-based statistics. This fact depends on the quality of the gyroscopes and should be accounted for when selecting the relative weighting between decision statistics. $M_{acc}[n]$ and $H_{acc}[n]$ assume very close values. This result is expected and reflects the validity of the assumption that the vehicle mostly moves in the horizontal plane.

The decision statistics computed for the SPAN-CPT when the GNSS and IMU data are from two different test runs are provided in Fig. 9. This case corresponds to a spoofing

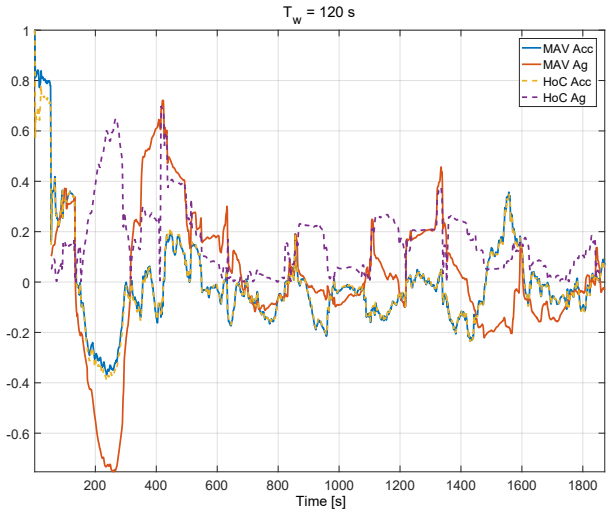

Fig. 9. Decision statistics computed for the SPAN-CPT when the GNSS and IMU data are from two different test runs.

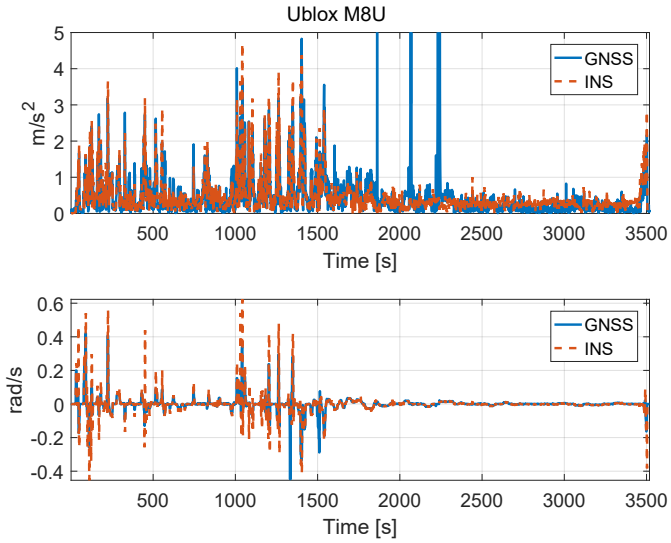

Fig. 10. Comparison between time series obtained using the HoC approach. Upper part) Horizontal acceleration. Bottom part) Angular velocity. ublox M8U experiment, genuine scenario.

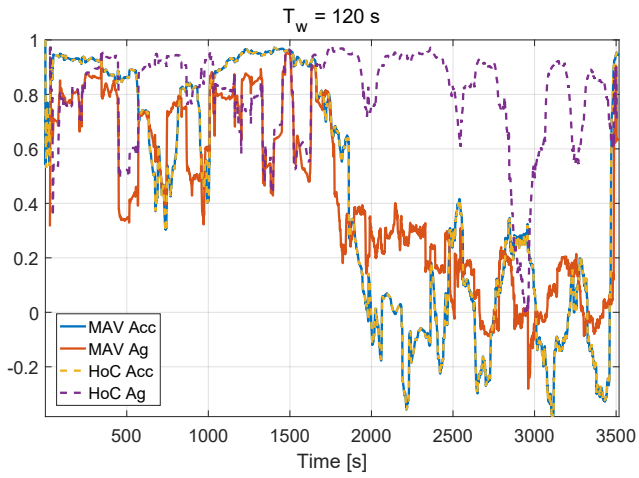

Fig. 11. Decision statistics computed for the ublox M8U scenario analysed in Fig. 10.

scenario where GNSS data are falsified. In this case, the correlation coefficients assume values lower than 0.6. Higher values are sporadically observed either because of portion of data of constant velocity or for coincident turns, i.e. when the vehicle perform similar turns in both test runs. It is noted that the datasets used for the computation of the test statistics in Fig. 9 were obtained by considering the same trajectory. Even if the data are not synchronized, similar manoeuvres can occur. Thus, the results shown in Fig. 9 can be considered as pessimistic. It is also noted that high correlation values are not observed simultaneously in both acceleration and angular velocity decision statistics. These results show the effectiveness of the decision statistics to distinguish genuine and spoofing cases when high quality IMU data are used.
These results also suggest that for this type of IMU, a decision threshold around 0.7 can be adopted to discriminate between normal and spoofing conditions. The threshold however depends to the specific IMU and on the parameters used for the computation of the decision statistics.

B. Ublox M8U

Results obtained using the ublox M8U device are provided in Fig. 10 that compares the time series obtained using the HoC approach. As for the SPAN-CPT case, an overall good agreement between time series is observed. The test considered in Fig. 10 corresponds to the trajectory shown in Fig. 6c) and was performed mostly in a highway scenario. During the second part of the test, after about 1500 seconds from the start, the driver was asked to maintain a steady velocity and to avoid lane changes. This fact clearly emerges from the time series shown in Fig. 10. Low accelerations and angular velocities are recorded during this part of the test. This driving behavior corresponds to the worst case scenario for the verification strategies considered in this paper. Low accelerations and angular velocities are difficult to cross-check since noise components tend to dominate.
The decision statistics obtained for this scenario are analysed in Fig. 11. The two parts of the test can be clearly identified: higher correlation values are observed during the first part of the test when the driver is maintaining a less constant behavior. The $H_{ag}[n]$ decision static is the less affected by low dynamic changes and it scores high correlation values even during the second part of the test. This is due to the fact that $H_{ag}[n]$ is computed from the horizontal angular velocity where both magnitude and sign information are used. Even if the magnitude of the angular velocity is small, sign variations correlate well between GNSS and IMU time series. $M_{ag}[n]$ seems to be the most affected by low dynamic changes and the usage of $H_{ag}[n]$ should be preferred. The presence of notches in the $H_{ag}[n]$ time series can be compensated by introducing verification strategies or considering larger analysis windows. The decision statistics computed for the ublox M8U device when the GNSS and IMU data are from two different tests are shown in Fig. 12. The results are similar to those obtained for the SPAN-CPT case. The decision statistics assume value below 0.6 with occasional spikes with higher values. These

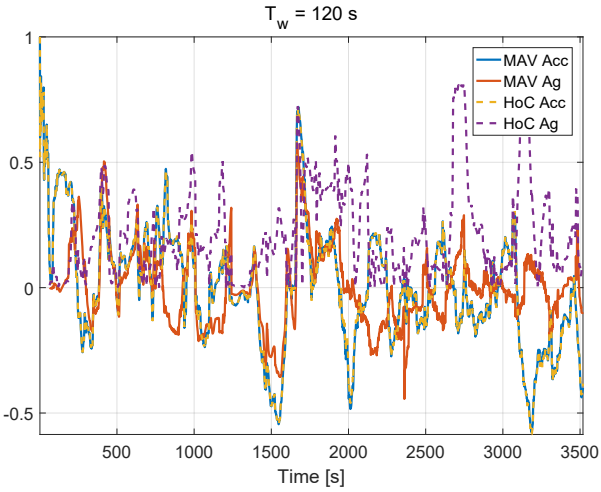

Fig. 12. Decision statistics computed for the ublox M8U when the GNSS and IMU data are from two different tests.

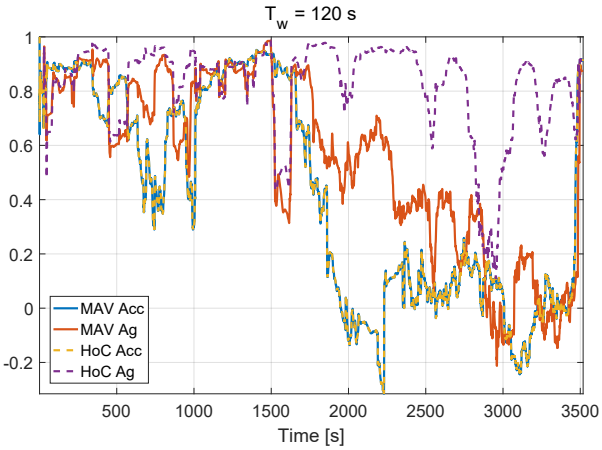

Fig. 13. Decision statistics computed for the Huawei P10 data obtained from the scenario analysed in Fig. 10.

values highlight the need for verification strategies where the choice between genuine and spoofing conditions is based on decision statistics from several epochs.

C. Huawei P10

The results obtained using the data collected using the Huawei P10 phone are shown in Fig. 13 that provides the decision statistics obtained for the same scenario considered for the ublox M8U device. The results obtained are very similar to those found for the ublox M8U device. The decision statistics follow a trend similar to that shown in Fig. 11. This shows the possibility of performing data verification using the low-cost IMU integrated in a smartphone.

D. Huawei G Play Mini

Finally, results obtained using data from the Huawei G Play Mini are analysed. The data analysed here are from a different test with respect to the experiment considered in the previous sections. In the experiment considered above, the Huawei G Play Mini was not available. The data provided by this low-end phone are too poor and a low correlation is found between

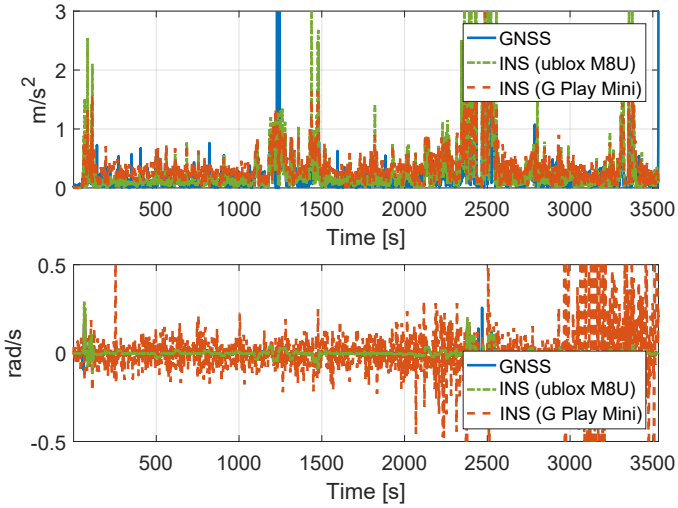

Fig. 14. Comparison between time series obtained using the HoC approach. Upper part) Horizontal acceleration. Bottom part) Angular velocity. Huawei G Play Mini and ublox M8U devices, genuine scenario.

GNSS and inertial data as shown in Fig. 14 that provides the time series obtained using the HoC approach. While it is possible to observe a common trend between the horizontal acceleration time series, the horizontal angular velocity from the phone gyroscopes is too noisy and cannot be used for data verification. In this case, the approaches proposed cannot be used. The figure also shows the data obtained using the measurements from the ublox M8U device. In the ublox M8U case, a good agreement between GNSS and INS data is found.

V. Discussion

From the analysis performed in previous sections, it emerged that, under particular conditions, the approach proposed may be ineffective. Some considerations on possible causes and improvements are discussed in the following.

A. Zero Velocity Detection

When the vehicle is static, the decision statistics analysed become ineffective and a different approach should be used. In particular, zero velocity detection should be implemented and start/stop periods should be recorded. It is then possible to verify that both GNSS and IMU sensors have recorded the same static periods. Several approaches exist in the literature for zero velocity detection [15]. While they have been mainly developed for pedestrian navigation, they can be easily adapted to the automotive sector, for example, by incorporating the model assumptions discussed in Section II.

It is noted that long zero velocity conditions occur when the vehicle driver is resting. The respect of rest periods is important for road safety and the ST regulations prescribe the periodic verification of driving pauses [3]. In traffic conditions, the continuous transitions between static and dynamic conditions can lead to strong signatures for spoofing detection. For these reasons, the approaches considered here should be integrated in a more complex decision logic where zero velocity detection should play a significant role.

B. Outlier Removal and Data Smoothing

Figs. 10 and 14 sporadically show spikes and impulsive features that are often present only in one time series. Similar effects can be observed in [9] where data from a high end smartphone were used. These spikes may significantly bias the correlation values used as decision statistics. For this reason, outlier removal and data smoothing should be implemented. A median filter [16] is effective in removing outliers, however the selection of the appropriate length of the filter is an open problem and depends on the quality of the sensors used for the data collection. An excessive length of the analysis window of the median filter can lead to the removal of important features that would provide high correlation values.

C. Adaptive Decision Statistic Weighting

In [9], the final decision was taken by linearly combining the decision statistics computed from the accelerometer and from the gyroscope measurements. A fixed constant was used for the combination. In the experiments conducted here, it was shown that, depending on the dynamic conditions of the vehicle, a decision statistic can be more effective than another in determining data correlation. In Fig. 11 it is shown that the $H_{ag}[n]$ is the most effective decision statistic when low dynamic changes occur. For this reason, the final decision statistics,

$$\begin{aligned} M[n] &= (1-\alpha)M_{acc}[n] + \alpha M_{ag}[n] \\ H[n] &= (1-\alpha)H_{acc}[n] + \alpha H_{ag}[n], \end{aligned} \tag{15}$$

should be determined using an adaptive approach. The weight, α, should be selected according to the vehicle dynamics and to the level of acceleration and angular velocity measured by the different sensors.

VI. Conclusions

In this paper, GNSS/IMU uncoupled verification strategies were considered and analysed from an experimental point of view. A modified strategy that requires levelling was developed and an approach based on the horizontal angular velocity was proposed.

From the analysis, it emerges that IMU measurements can be used to verify GNSS information even when data from smartphones are used. The smartphones however have to be of sufficient quality to provide reliable angular velocity information. The tests performed show that the horizontal angular velocity provides the most reliable information when low vehicle dynamics are experienced. This is due to the fact that approaches based on the measurement magnitude lose direction information that is fundamental for correlation purposes. The analysis also shows the limit of these data verification strategies and the need for integrated approaches that implement zero velocity detection, outlier removal and adopt an adaptive behaviour depending on the vehicle dynamics.

References

[1] M. L. Psiaki and T. E. Humphreys, "GNSS spoofing and detection," *Proc. IEEE*, vol. 104, no. 6, pp. 1258–1270, Jun. 2016.

[2] G. Baldini, L. Sportiello, M. Chiaramello, and V. Mahieu, "Regulated applications for the road transportation infrastructure: The case study of the smart tachograph in the european union," *International Journal of Critical Infrastructure Protection*, vol. 21, pp. 3 – 21, 2018. [Online]. Available: http://www.sciencedirect.com/science/article/pii/S1874548217300392

[3] European Parliament and European Council, "Regulation (EU) No 799/2016 of the European Parliament and of the Council of 18th March 2016 on the requirements for the construction, testing, installation, operation and repair of tachographs and their components," on-line, 2016, http://eur-lex.europa.eu/legal-content/EN/TXT/PDF/?uri=CELEX:32016R0799.

[4] D. Borio, E. Cano, and G. Baldini, "Speed consistency in the smart tachograph," *Sensors*, vol. 18, no. 5, pp. 1–21, May 2018.

[5] A. Broumandan and G. Lachapelle, "Spoofing detection using GNSS/INS/Odometer coupling for vehicular navigation," *Sensors*, vol. 18, no. 5, pp. 1–18, May 2018.

[6] S. Manickam and K. O'Keefe, "Using tactical and MEMS grade INS to protect against GNSS spoofing in automotive applications," in *Proc. of the 29th International Technical Meeting of The Satellite Division of the Institute of Navigation (ION GNSS+)*, Portland, Oregon, Sep. 2016, pp. 2991–3001.

[7] C. Tanil, S. Khanafseh, and B. Pervan, "An INS monitor against GNSS spoofing attacks during GBAS and SBAS-assisted aircraft landing approaches," in *Proc. of the 29th International Technical Meeting of the ION Satellite Division, ION GNSS+*, Portland, Oregon, Sep. 2016, pp. 2981–2990.

[8] S. Lo, Y. H. Chen, T. Reid, A. Perkins, T. Walter, and P. Enge, "The benefit of low cost accelerometers for GNSS anti-spoofing," in *Proc. of the ION Pacific PNT Meeting*, Honolulu, Hawaii, May 2017, pp. 775–796.

[9] J. T. Curran and A. Broumendan, "On the use of low-cost IMUs for GNSS spoofing detection in vehicular applications," in *Proc. of the International Technical Symposium on Navigation and Timing (ITSNT)*, Toulouse, France, Nov. 2017, pp. 1–8.

[10] D. G. Abby, *Global Positioning System Theory and Applications*, ser. Progress in Astronautics and Aeronautics. Reston, VA: American Institute of Aeronautics & Astronautics, 1996, vol. 2, ch. Ch 22, Test Range Instrumentation, pp. 593–624.

[11] A. K. Bourke, K. O'Donovan, A. Clifford, G. Ólaighin, and J. Nelson, "Optimum gravity vector and vertical acceleration estimation using a tri-axial accelerometer for falls and normal activities," in *Annual International Conference of the IEEE Engineering in Medicine and Biology Society*, Aug. 2011, pp. 7896–7899.

[12] S. O. H. Madgwick, A. J. L. Harrison, and R. Vaidyanathan, "Estimation of IMU and MARG orientation using a gradient descent algorithm," in *IEEE International Conference on Rehabilitation Robotics*, Jun. 2011, pp. 1–7.

[13] J. F. Vasconcelos, B. Cardeira, C. Silvestre, P. Oliveira, and P. Batista, "Discrete-time complementary filters for attitude and position estimation: Design, analysis and experimental validation," *IEEE Trans. Control Syst. Technol.*, vol. 19, no. 1, pp. 181–198, Jan 2011.

[14] S. O. Haykin, *Adaptive Filter Theory*, 5th ed. Pearson, Jun. 2013.

[15] I. Skog, P. Händel, J.-O. Nilsson, and J. Rantakokko, "Zero-velocity detectionan algorithm evaluation," *IEEE Trans. Biomed. Eng.*, vol. 57, no. 11, pp. 2657–2666, Nov. 2010.

[16] G. R. Arce, *Nonlinear Signal Processing: A Statistical Approach*. Wiley-Interscience, Nov. 2004.

Daniele Borio received the doctoral degree in electrical engineering from Politecnico di Torino, Italy in April 2008. He is a scientific technical officer at the Joint Research Centre of the European Commission, Ispra, Italy. His research interests include the fields of digital and wireless communications, location, and navigation.